Analysis and design of an Extended Kalman Filter for the plate temperature in heavy plate rolling

authored by **K. Speicher, A. Steinboeck, A. Kugi, D. Wild, T. Kiefer**

and published in *Journal of Process Control*.

```
@Article{acinpaper,
  Title = {Analysis and design of an {E}xtended {K}alman {F}ilter for the plate temperature in heavy plate
      rolling},
  Author = {Speicher, K. and Steinboeck, A. and Kugi, A. and Wild, D. and Kiefer, T.},
  Journal = {Journal of Process Control},
  Year = {2014},
  Number = {9},
  Pages = {1371--1381},
  Volume = {24},
  Doi = {10.1016/j.jprocont.2014.06.004},
  Url = {http://www.sciencedirect.com/science/article/pii/S095915241400167X#}
}
```

Contact:

Automation and Control Institute (ACIN)
Vienna University of Technology
Gusshausstrasse 27-29/E376
1040 Vienna, Austria

Internet: www.acin.tuwien.ac.at
E-mail: office@acin.tuwien.ac.at
Phone: +43 1 58801 37601
Fax: +43 1 58801 37699

Analysis and design of an Extended Kalman Filter for the plate temperature in heavy plate rolling

K. Speicher[a,*], A. Steinboeck[a], A. Kugi[a], D. Wild[b], T. Kiefer[b]

[a]*Automation and Control Institute, Vienna University of Technology, Vienna, Austria*
[b]*AG der Dillinger Hüttenwerke, Dillingen, Germany*

Abstract

This paper deals with the estimation of the plate temperature in heavy plate rolling. An Extended Kalman Filter (EKF) is designed and its initialization and parametrization are discussed in detail. The observer is validated by means of experimental data recorded during a measurement campaign with a special developed test plate instrumented with thermocouples. It is shown that a good estimation accuracy can be achieved under normal production conditions despite the scarcity of measurements. Furthermore, the coupling effect between the plate and the work rolls is investigated in more detail. Based on this analysis, the validity of a computationally inexpensive reduced observer is demonstrated.

Keywords: Extended Kalman Filter, heavy plate hot rolling, temperature control, temporarily coupled systems, switched system, parameter estimation

1. Introduction

The quality demands in the steel industry are steadily increasing. Thus, the production process of steel plates has to be controlled precisely. For example, it is vital that the rolling takes place in the prescribed temperature range. Therefore, the temperature evolution of the plates has to be considered carefully when planning the roll pass schedule. The plate temperature is influenced by many factors during the production process. Air cooling periods during transport and waiting times, descaling passes, and roll passes alternate and expose the plate to different modes of heat transfer. On the one hand, heat is lost due to the contact with the cold work rolls, by radiation or because of the thermal shock caused by the descaler sprays. On the other hand, the deformation during the roll passes leads to a temperature rise. These effects have to be captured by a thermal model. Numerous thermal models are given in the literature, e. g., [1, 2, 3, 4, 5, 6].

Model inaccuracies, wrong parameters of the plate itself (e. g., material parameters), or changes in the rough production conditions may result in wrong predictions of the temperature. To improve the prediction quality, observers can be designed which make use of the temperature measurements recorded during the production process. However, in general, only pyrometer measurements of the surface temperature are available, the temperature distribution inside the plate cannot be measured. Furthermore, the pyrometers measure only infrequently, when the plate passes the pyrometer. Consequently, the observer has not only to cope with the switched system structure caused by the alternating production steps, but it must also handle rare and infrequent measurements.

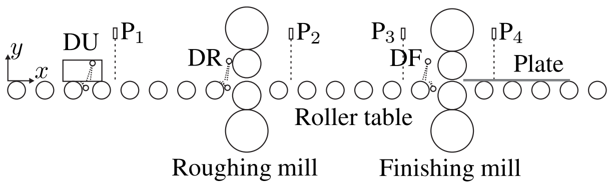

Figure 1: Overview of the considered rolling mill (DU: descaler unit; DR: descaler sprays roughing mill; DF: descaler sprays finishing mill; P_1-P_4: pyrometers.

Observers for the plate temperature were developed by, e. g., [7, 8]. However, these observers require measurements of temperatures or other states, e. g., the plate thickness, after each pass. This is not possible in the considered rolling mill of AG der Dillinger Hüttenwerke, which is schematically depicted in Fig. 1. During the roll passes at the roughing mill, the plate is too short to pass the pyrometers, which are at a distance of approximately 8 m from the mill stand because of the difficult measurement conditions closer to the mill stand. Transporting the plate to these pyrometers between two roll passes would cause delays in the production schedule. The observer presented in [9] even uses continuous measurements which are available in strip rolling, but not in plate rolling. Furthermore, the cited publications focus mainly on a single production step, e. g., a roll pass, instead of the whole production process with alternating production steps. Observers for switched systems, which can handle a sequence of different production steps, are presented in, e. g., [10, 11], but they also require continuous measurements. The scarcity of measurements also poses a

*Corresponding author at: Automation and Control Institute, Vienna University of Technology, Gusshausstrasse 27-29, 1040 Vienna, Austria.
Tel.: +43 1 58801 37628, fax: +43 1 58801 37699
Email address: speicher@acin.tuwien.ac.at (K. Speicher)

Post-print version of the article: K. Speicher, A. Steinboeck, A. Kugi, D. Wild, T. Kiefer, "Analysis and design of an Extended Kalman Filter for the plate temperature in heavy plate rolling", *Journal of Process Control*, 24, 9, 1371–1381, 2014. DOI: 10.1016/j.jprocont.2014.06.004
The content of this post-print version is identical to the published paper but without the publisher's final layout or copy editing.

problem in bioprocess applications, where Extended Kalman Filter (EKF) are widely used as observers, see, e. g., [12, 13]. The performance of the EKF depends strongly on some tuning factors and there is no consensus about a simple and general-purpose way to choose them for all kind of systems, see, e. g., [14, 15].

In this paper, an Extended Kalman Filter is designed for the considered switched system with infrequent measurements. The tuning factors are systematically chosen based on an analysis of the model and the underlying production process. In Section 2, an existing thermal model of the plate is shortly reviewed and extended by a thermal model of the work rolls. The main part of this work, Section 3, deals with the design of the EKF. In Section 4, the EKF is validated by means of experimental data recorded during a measurement campaign with a special test plate. Furthermore, the coupling effect between the plate and the work rolls is investigated using measurement data from the production of a standard plate. At the end, conclusions are drawn and an outlook on future work is given in Section 5.

2. Mathematical model

In this paper, a rolling mill with two four-high reversing mill stands is considered, see Fig 1. From the exit of an upstream slab reheating furnace to the last roll pass at the finishing mill, mainly the three already mentioned influences on the temperature evolution of the plate have to be modeled: the air cooling during transport and waiting periods, the thermal shock caused by the descaler sprays, and the roll passes themselves. A thermal model of the plate that captures all these aspects was developed in [1]. In the following, the existing thermal model is extended by a work roll model.

2.1. Plate model

The thermal model of the plate calculates the time evolution of a vertical temperature profile in the main part of the plate. A one-dimensional heat conduction equation through the thickness is considered with different boundary conditions for the different submodels, i. e., air cooling, descaling, and rolling. The partial differential equation is discretized by means of the finite difference method using a spatial grid with varying mesh size. The used grid is coarse in the core of the plate and fine close to its surfaces. The total number of grid points depends on the current plate thickness and amounts to up to 100. Central difference quotients of second order approximate the spatial partial derivative at the grid points. The backward Euler method is used for time discretization. The resulting model takes the form [1]

$$\mathbf{f}_j^{\mathrm{p}}(\mathbf{x}_{j+1}^{\mathrm{p}}, \mathbf{x}_j^{\mathrm{p}}, \mathbf{u}_{j+1}) = \mathbf{0}, \tag{1}$$

with the state vector $\mathbf{x}_j^{\mathrm{p}} = \left[T_j^{\mathrm{p},1} \dots T_j^{\mathrm{p},N}\right]^T$ comprising the temperatures $T_j^{\mathrm{p},i} = T_j^{\mathrm{p}}(y_i, t_j)$ at the plate's grid points y_i at time t_j. The lower and the upper surface temperature, $T^{\mathrm{p},1}$ and $T^{\mathrm{p},N}$, respectively, are also referred to as $T_{\mathrm{lo}}^{\mathrm{p,s}}$ and $T_{\mathrm{up}}^{\mathrm{p,s}}$. The superscript "s" is used to denote surface temperatures, while "c" designates the core temperature. During roll passes, the state vector has to be extended by the temperatures at the grid points of both work rolls. Moreover, $\mathbf{u}_{j+1}$ contains all remaining terms that do not depend on the states but rather on parameters, e. g., the water temperature, the geometry of the roller table, or the heat transfer coefficients. For more details, the reader is referred to [1].

2.2. Work roll model

As already mentioned, the thermal model (1) captures the temperature evolution of the work rolls only during the short contact time with the plate. The contact takes place in the zone A indicated in Fig. 2 and accounts for only a small portion of a complete revolution of the work roll. In the following, a model of the temperature evolution of the work roll in the remaining zones is presented.

In the work rolls, the heat flows mainly in radial direction if the angular speed of the work roll is sufficiently large. Hence, the one-dimensional heat conduction equation in cylindrical coordinates can be considered, i. e.,

$$\begin{gathered}\rho_{\mathrm{wr}}(r)c_{\mathrm{wr}}(r)\frac{\partial T^{\mathrm{wr}}(r,t)}{\partial t} = \frac{1}{r}\frac{\partial}{\partial r}\left(r\lambda_{\mathrm{wr}}(r)\frac{\partial T^{\mathrm{wr}}(r,t)}{\partial r}\right),\\ r \in (R-\delta_r, R), \quad t > 0\end{gathered} \tag{2}$$

with the temperature T^{wr} of the work roll and appropriate initial conditions. The material properties, i. e., the density ρ_{wr}, the heat capacity c_{wr}, and the thermal conductivity λ_{wr}, are assumed to be independent of the temperature. They depend on the radial coordinate r because the work rolls consist of different materials in the core and the shell. As the cyclic heating and cooling of the work rolls is confined to a thin boundary layer of thickness δ_r, the heat conduction equation (2) is only solved for the spatial domain $r \in (R-\delta_r, R)$. The core of the work roll, $r < R - \delta_r$, is assumed to be at constant temperature. Consequently, the heat flux equals zero at the inner boundary, i. e.,

$$\dot{q}_{\mathrm{wr,in}} = \lambda_{\mathrm{wr}}(r)\frac{\partial T^{\mathrm{wr}}(r,t)}{\partial r}\bigg|_{r=R-\delta_r} = 0. \tag{3}$$

To specify the boundary condition at the outer boundary, $r = R$, a revolution of the work roll has to be analyzed. During one revolution in a roll pass, a point on the surface of the work roll moves through zones with different boundary conditions. Consequently, the heat flux leaving the work roll depends on the current zone, i. e.,

$$\begin{gathered}\dot{q}_{\mathrm{wr,out}} = -\lambda_{\mathrm{wr}}(r)\frac{\partial T^{\mathrm{wr}}(r,t)}{\partial r}\bigg|_{r=R} = \dot{q}_{\mathrm{wr},k}\\ k \in \{A, B, C, D, E\}.\end{gathered} \tag{4}$$

These zones are indicated in Fig. 2 and specified in the following:

- *Contact with the plate (A)*: The heat flux $\dot{q}_{\mathrm{wr,A}}$ at the work roll/plate interface is composed of two parts due to conduction and friction, see [1]. As the work rolls are much colder than the plate, the heat flows from the plate to the work roll. The thermal effect of friction in the roll gap can be modeled in the form of a surface heat source.

Post-print version of the article: K. Speicher, A. Steinboeck, A. Kugi, D. Wild, T. Kiefer, "Analysis and design of an Extended Kalman Filter for the plate temperature in heavy plate rolling", *Journal of Process Control*, 24, 9, 1371–1381, 2014. doi: 10.1016/j.jprocont.2014.06.004
The content of this post-print version is identical to the published paper but without the publisher's final layout or copy editing.

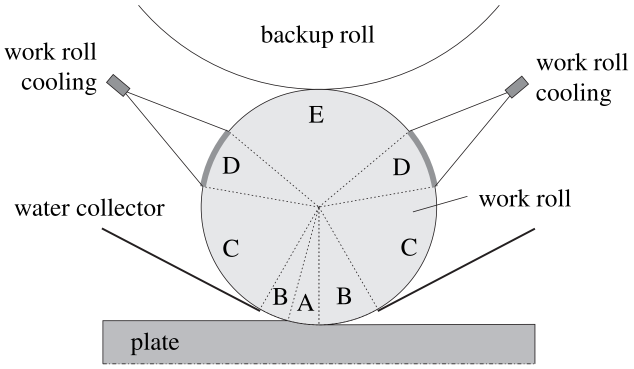

Figure 2: Boundary conditions of the work roll.

- *Radiative heat exchange with the plate (B)*: Assuming that the view factor between the plate and the work roll is 1, the net radiation method, see [16], yields

$$\dot{q}_{\mathrm{wr,B}} = \sigma \frac{\varepsilon^{\mathrm{p}} \varepsilon^{\mathrm{wr}}}{\varepsilon^{\mathrm{wr}} + \varepsilon^{\mathrm{p}} - \varepsilon^{\mathrm{wr}} \varepsilon^{\mathrm{p}}} \left((T^{\mathrm{wr,s}})^4 - (T^{\mathrm{p,s}})^4 \right), \qquad (5)$$

  where $T^{\mathrm{wr,s}}$ and $T^{\mathrm{p,s}}$ denote the surface temperatures of the work roll and the plate, respectively. Moreover, $\varepsilon^{\mathrm{wr}}$ and ε^{p} are the respective emissivities and σ is the Stefan–Boltzmann constant. The heat flux (5) is usually negative because the plate is warmer than the work roll. By definition, negative heat fluxes enter the work roll at its boundary.

- *Impact area of the cooling sprays (D), film of cooling water (C)*: Modeling the heat transfer is a difficult task in the impact areas of the cooling sprays and in the zones with a water film streaming downwards from the spray zones. The mode of heat transfer varies depending on the current surface temperature and may be, e. g., natural convection, film boiling, or nucleate boiling. For simplicity reasons, convective boundary conditions of the form

$$\dot{q}_{\mathrm{wr},k} = h_{\mathrm{wr},k}(T^{\mathrm{wr,s}} - T_{\mathrm{w}}), \quad k \in \{\mathrm{C}, \mathrm{D}\}, \qquad (6)$$

  are used in this work. The heat transfer coefficients are chosen according to [17], i. e., $h_{\mathrm{wr,D}} = 8300\,\mathrm{W/(m^2\,K)}$ and $h_{\mathrm{wr,C}} = 850\,\mathrm{W/(m^2\,K)}$. T_{w} denotes the constant water temperature.

- *Area of influence of the backup roll (E)*: It is assumed that the heat flux in this zone is mainly determined by the film of cooling water streaming down from the backup rolls. However, the mechanical contact with the cold backup rolls may also contribute to the heat loss. Therefore, the heat transfer coefficient in (6) is chosen slightly higher than in zone C, that is $h_{\mathrm{wr,E}} = 1000\,\mathrm{W/(m^2\,K)}$.

When calculating the work roll temperature evolution, the outer boundary condition switches whenever the considered point on the surface of the work roll enters a new zone.

Between two passes, the boundary conditions in zones C to E remain unchanged because the spray cooling works permanently. On the contrary, in zones A and B, radiative heat exchange between the two work rolls and the roller table has to be considered instead of the interaction with the plate. The resulting heat flux is calculated by (5) replacing $T^{\mathrm{p,s}}$ and ε^{p} by the constant temperature T_{r} of the roller table and its emissivity ε_{r}, respectively.

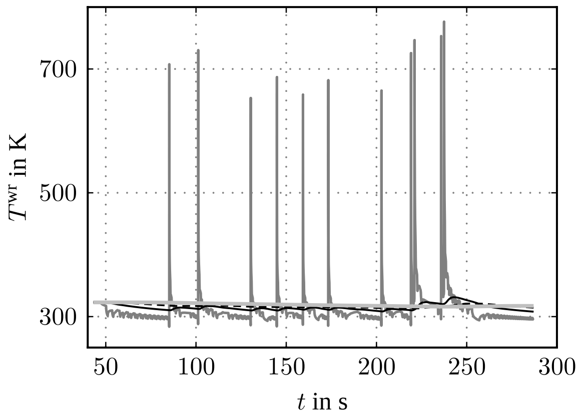

(a) Work roll at the roughing mill.

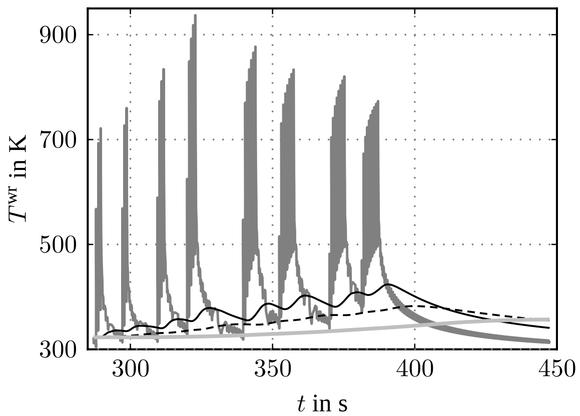

(b) Work roll at the finishing mill.

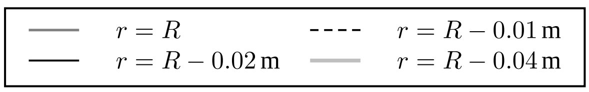

Figure 3: Work roll temperatures during the production of a standard plate.

Figs. 3a and 3b show the evolution of a radial temperature profile of the work rolls at the roughing and the finishing mill, respectively. The temperature of each work roll is shown in the relevant time period, i. e., during the roll passes at the respective mill stand. During the remaining time, the work rolls are cooled by the water sprays.

Starting from a homogeneous temperature $T^{\mathrm{wr}}(r) = 323\,\mathrm{K}$, the surface temperature (dark gray solid line) heats up quickly during the first pass at the roughing mill, but descends again to approximately room temperature due to the water cooling. Later in the production process, when the plate is so long that a pass consists of several revolutions of the work roll, i. e., from the eighth roll pass on, the work roll surface temperature stays

Post-print version of the article: K. Speicher, A. Steinboeck, A. Kugi, D. Wild, T. Kiefer, "Analysis and design of an Extended Kalman Filter for the plate temperature in heavy plate rolling", *Journal of Process Control*, 24, 9, 1371–1381, 2014. DOI: 10.1016/j.jprocont.2014.06.004
The content of this post-print version is identical to the published paper but without the publisher's final layout or copy editing.

elevated between the passes. However, the resulting heat conduction from the surface to the core of the work roll influences only a thin surface layer ($r > R - 5\,\mathrm{cm}$). Therefore, the choice $\delta_r = 5\,\mathrm{cm}$ in Eq. (2) is justified.

2.3. Extended model

The thermal model from [1] is extended by the discretized work roll model developed in Section 2.2. The resulting implicit formulation of the model has the same form as Eq. (1), i. e.,

$$\mathbf{f}_j(\mathbf{x}_{j+1}, \mathbf{x}_j, \mathbf{u}_{j+1}) = \mathbf{0}. \tag{7}$$

The state vector $\mathbf{x}_j = \left[\left(\mathbf{x}_j^{\mathrm{wr,lo}}\right)^T \left(\mathbf{x}_j^{\mathrm{p}}\right)^T \left(\bar{\mathbf{x}}_j^{\mathrm{wr,up}}\right)^T\right]^T$ contains the grid point temperatures of the two work rolls, $\mathbf{x}_j^{\mathrm{wr,lo}}$ and $\bar{\mathbf{x}}_j^{\mathrm{wr,up}}$, and those of the plate $\mathbf{x}_j^{\mathrm{p}}$. The temperatures $\mathbf{x}_j^{\mathrm{wr,lo}}$ of the lower work roll are given from the core to the surface, whereas those of the upper work roll $\bar{\mathbf{x}}_j^{\mathrm{wr,up}}$ are arranged in the opposing direction (indicated by the bar superscript). This arrangement is advantageous when linearizing the nonlinear system (7) in the course of the derivation of the Extended Kalman Filter.

The extended model captures all significant influences on the temperature of the plate and the work rolls from the exit of the slab reheating furnace to the last roll pass at the finishing mill. During the roll passes, the plate and the work rolls are thermally coupled, whereas their temperature evolutions are decoupled between the passes. Furthermore, the boundary conditions depend on the current production step and on the current kinematic state of the work rolls (rotation angle, angular speed). Consequently, the whole system consists of three temporarily coupled switched systems, i. e., the plate and the two work rolls.

Remark: As the emissivity of the plate also strongly influences the temperature evolution of the plate, but varies during the production, it should be estimated and updated online. To estimate the slowly varying emissivity, the model (7) is extended by the trivial dynamic equation

$$\varepsilon_{j+1}^{\mathrm{p}} = \varepsilon_j^{\mathrm{p}}. \tag{8}$$

The state vector is then $\mathbf{x}_j = \left[\left(\mathbf{x}_j^{\mathrm{wr,lo}}\right)^T \left(\mathbf{x}_j^{\mathrm{p}}\right)^T \left(\bar{\mathbf{x}}_j^{\mathrm{wr,up}}\right)^T \varepsilon_j^{\mathrm{p}}\right]^T$.

3. Observer design

Based on the model presented in Section 2, an observer is developed. It uses the measurements of the surface temperatures of the plate that are recorded by several pyrometers. In the considered rolling mill, a total of 12 pyrometers (11 top-side, one bottom-side) are placed along the production line, which has a length of about 200 m. The four pyrometers indicated in Fig. 1 are the most important ones for the observer. Thus, only few and infrequent measurements are available because the pyrometers are mounted at fixed positions and only measure at times when the plate passes by. Furthermore, there might be an unknown delay until the measurement becomes available due to the time needed for signal processing. Different ways to handle infrequent, randomly sampled or delayed measurements are given in [18, 19, 20]. In the case considered here, the delay can be neglected for reasons that are discussed in Section 3.3. Therefore, an Extended Kalman Filter (EKF) for continuous-time systems with discrete-time measurements is presented in the following section.

3.1. Extended Kalman Filter

Prior to the observer design, the extended system (7) according to Section 2.3 is augmented by the process noise $\mathbf{w}_j$ and the measurement noise $\mathbf{v}_j$ resulting in

$$\begin{aligned} \mathbf{f}_j(\mathbf{x}_{j+1}, \mathbf{x}_j, \mathbf{u}_{j+1}) + \mathbf{w}_j &= \mathbf{0} \\ \mathbf{z}_j &= \mathbf{h}_j(\mathbf{x}_j) + \mathbf{v}_j, \end{aligned} \tag{9}$$

with the measured quantity $\mathbf{z}_j$ and the nonlinear measurement function $\mathbf{h}_j(\mathbf{x}_j)$ to be discussed in Section 3.3. Here, $\mathbf{w}_j$ and $\mathbf{v}_j$ are assumed to be normally distributed white noise sequences with zero mean and positive definite covariance matrices $\mathbf{Q}_j$ and $\mathbf{R}_j$, respectively.

The EKF consists of two computational steps, i. e., the *corrector step* and the *predictor step*. In the corrector step, the measurement $\mathbf{z}_j$ is used to correct the so-called a priori estimation $\hat{\mathbf{x}}_j^-$ of the state vector. This correction update is only possible if a measurement is available at time t_j. The corrected estimation, the so-called a posteriori estimation $\hat{\mathbf{x}}_j^+$, is calculated by

$$\hat{\mathbf{x}}_j^+ = \hat{\mathbf{x}}_j^- + \hat{\mathbf{L}}_j\left(\mathbf{z}_j - \mathbf{h}_j(\hat{\mathbf{x}}_j^-)\right) \tag{10}$$

with the Kalman gain

$$\hat{\mathbf{L}}_j = \mathbf{P}_j^-\mathbf{C}_j^T\left(\mathbf{C}_j\mathbf{P}_j^-\mathbf{C}_j^T + \mathbf{R}_j\right)^{-1}. \tag{11}$$

The matrix $\mathbf{C}_j$ is defined by $\mathbf{C}_j = \left.\frac{\partial \mathbf{h}_j}{\partial \mathbf{x}_j}\right|_{\mathbf{x}_j=\hat{\mathbf{x}}_j^-}$. The covariance matrix $\mathbf{P}_j^- = E\left(\left(\hat{\mathbf{x}}_j^- - \mathbf{x}_j\right)\left(\hat{\mathbf{x}}_j^- - \mathbf{x}_j\right)^T\right)$ of the estimation error is corrected in the form

$$\mathbf{P}_j^+ = \left(\mathbf{I} - \hat{\mathbf{L}}_j\mathbf{C}_j\right)\mathbf{P}_j^-, \tag{12}$$

with the identity matrix $\mathbf{I}$.

In the predictor step, the a posteriori estimation $\hat{\mathbf{x}}_j^+$ is extrapolated according to the system dynamics

$$\mathbf{f}_j\left(\hat{\mathbf{x}}_{j+1}^-, \hat{\mathbf{x}}_j^+, \mathbf{u}_{j+1}\right) = \mathbf{0}. \tag{13}$$

To calculate the extrapolated covariance matrix $\mathbf{P}_{j+1}^-$ of the estimation error, the system is linearized at the point $\diamond \mathrel{\hat{=}} \{\mathbf{x}_{j+1} = \hat{\mathbf{x}}_{j+1}^-, \mathbf{x}_j = \hat{\mathbf{x}}_j^+\}$. When the linear system matrices

$$\mathbf{\Phi}_j = -\left(\left.\frac{\partial \mathbf{f}_j}{\partial \mathbf{x}_{j+1}}\right|_\diamond\right)^{-1} \left.\frac{\partial \mathbf{f}_j}{\partial \mathbf{x}_j}\right|_\diamond \tag{14a}$$

$$\mathbf{G}_j = -\left(\left.\frac{\partial \mathbf{f}_j}{\partial \mathbf{x}_{j+1}}\right|_\diamond\right)^{-1} \tag{14b}$$

are calculated, the advantage of the arrangement of the state

Post-print version of the article: K. Speicher, A. Steinboeck, A. Kugi, D. Wild, T. Kiefer, "Analysis and design of an Extended Kalman Filter for the plate temperature in heavy plate rolling", *Journal of Process Control*, 24, 9, 1371–1381, 2014. DOI: 10.1016/j.jprocont.2014.06.004
The content of this post-print version is identical to the published paper but without the publisher's final layout or copy editing.

vector according to Section 2.3 becomes evident: The matrix $\left.\frac{\partial \mathbf{f}_j}{\partial \mathbf{x}_{j+1}}\right|_{\diamond}$ is tridiagonal because central difference quotients of second order are used for discretization and the surface temperatures of the lower and upper work roll are placed close to the temperatures of the respective surfaces of the plate in the state vector. Thus, the matrix $\left.\frac{\partial \mathbf{f}_j}{\partial \mathbf{x}_{j+1}}\right|_{\diamond}$ can be inverted in an efficient way. Using the system matrices (14), $\mathbf{P}_{j+1}^{-}$ is obtained in the form

$$\mathbf{P}_{j+1}^{-} = \mathbf{\Phi}_j \mathbf{P}_j^{+} \mathbf{\Phi}_j{}^T + \mathbf{G}_j \mathbf{Q}_j \mathbf{G}_j{}^T. \tag{15}$$

Inserting Eq. (11) into Eq. (12) and the result into Eq. (15) yields a discrete-time Riccati equation. The choice of a suitable initial condition for this equation is discussed in the following section.

3.2. *Definition of initial conditions*

Before starting the estimation, initial conditions for the temperature profile $\hat{\mathbf{x}}_0$ and the covariance matrix $\mathbf{P}_0$ have to be specified. The initial temperature profile of the plate $\hat{\mathbf{x}}_0^{\mathrm{p}}$ is given by a model proposed in [21], which calculates the temperature profile of the plate at the exit of the reheating furnace. The two work rolls are assumed to be at a homogeneous temperature $T^{\mathrm{wr}}(r) = 323\,\mathrm{K}$.

Ideally, error covariances are transferred from observers of upstream production steps. If this is not possible, the covariance matrix is often initialized as a large multiple of the identity matrix. However, for the considered system, this choice proved inadequate because it does not take into account the coupling of neighboring grid point temperatures. As a consequence, the EKF does not use the first measurements of the surface temperature to correct the whole temperature profile. The correction only affects states close to the surface, see [22]. To capture the coupling between the grid point temperatures right from the beginning, the solution $\mathbf{P}_{\mathrm{stat}}^{\mathrm{p}}$ of the steady-state form

$$\mathbf{P}_{\mathrm{stat}}^{\mathrm{p}} = \mathbf{\Phi}_{\mathrm{stat}} \mathbf{P}_{\mathrm{stat}}^{\mathrm{p}} \mathbf{\Phi}_{\mathrm{stat}}^{T} + \mathbf{G}_{\mathrm{stat}} \mathbf{Q}_{\mathrm{stat}} \mathbf{G}_{\mathrm{stat}}^{T}, \tag{16}$$

of Eq. (15) is considered. As the system matrices in Eq. (15) are time variant, $\mathbf{\Phi}_{\mathrm{stat}}$, $\mathbf{G}_{\mathrm{stat}}$, and $\mathbf{Q}_{\mathrm{stat}}$ have to be chosen from a representative time step. Since no information about the system dynamics in the furnace is given, the system matrices of the air cooling submodel according to Eq. (14) at $t = 0$ are used in Eq. (16), i. e., $\mathbf{\Phi}_{\mathrm{stat}} = \mathbf{\Phi}_0$ and $\mathbf{G}_{\mathrm{stat}} = \mathbf{G}_0$. The covariance matrix of the process noise is also taken from the air cooling submodel, $\mathbf{Q}_{\mathrm{stat}} = \mathbf{Q}_0$. This matrix is defined in Section 3.4.

The algebraic matrix equation (16) has the form of a discrete-time Lyapunov matrix equation. Consequently, the existence of a unique positive definite matrix $\mathbf{P}_{\mathrm{stat}}^{\mathrm{p}}$ is guaranteed because $\mathbf{G}_0 \mathbf{Q}_0 \mathbf{G}_0{}^T$ is positive definite and $\mathbf{\Phi}_0$ is a contractive matrix. $\mathbf{P}_{\mathrm{stat}}^{\mathrm{p}}$ can serve as a reference for the coupling effect between the grid points but it has to be scaled to realistic values. Depending on the furnace, an estimation accuracy of 5 to 15 K is reasonable. Hence, $\mathbf{P}_0^{\mathrm{p}}$ is scaled so that its maximum element is $(15\,\mathrm{K})^2 = 225\,\mathrm{K}^2$.

Fig. 4 shows the resulting initial covariance matrix of the estimation error at the grid points of a slab with a thickness of 285 mm. The matrix elements are shown as a function of their grid point position. For example, the first row of $\mathbf{P}_0^{\mathrm{p}}$, which contains the elements $E(\Delta T_{\mathrm{lo},0}^{\mathrm{p,s}} \Delta \left(\mathbf{x}_0^{\mathrm{p}}\right)^T)$, can be seen on the border of the surface and corresponds to the grid points marked by the black line. The expectations of the squared estimation errors are given on the main diagonal of the matrix.

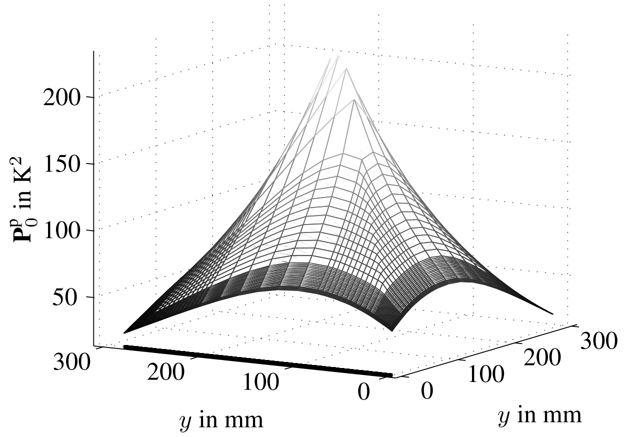

Figure 4: Initial covariance matrix $\mathbf{P}_0^{\mathrm{p}}$ of the estimation error of the plate temperature.

To find an appropriate initial covariance matrix of the estimation error of the work roll temperatures, a water cooling period is simulated starting from a homogeneous temperature profile and a diagonal covariance matrix. The resulting matrix at the end of this simulated cooling period is taken as $\mathbf{P}_0^{\mathrm{wr}}$.

The assembled initial covariance matrix has a block-diagonal structure and reads as

$$\mathbf{P}_0 = \begin{pmatrix} \mathbf{P}_0^{\mathrm{wr}} & \mathbf{0} & \mathbf{0} \\ \mathbf{0} & \mathbf{P}_0^{\mathrm{p}} & \mathbf{0} \\ \mathbf{0} & \mathbf{0} & \bar{\mathbf{P}}_0^{\mathrm{wr}} \end{pmatrix}. \tag{17}$$

Again, the bar superscript indicates the changed order of the states of the upper work roll (from the surface to the core).

3.3. *Measurement information*

When the plate passes a pyrometer, a longitudinal profile of the surface temperature is measured. However, the model (7) is one-dimensional and calculates only a temperature profile through the thickness which corresponds to the useful section of the plate. Therefore, only the measurement sequence corresponding to this section of the plate is fed into the EKF. Using the information about the motion of the plate, the respective measurement sequence of the surface temperature is detected and its mean value Θ_j and standard deviation σ_j are calculated.

It is known that the temperature measured by a pyrometer not only depends on the actual surface temperature of the considered object but also on its unknown radiation properties, see, e. g., [23] and the references given therein. As the exact relation

Post-print version of the article: K. Speicher, A. Steinboeck, A. Kugi, D. Wild, T. Kiefer, "Analysis and design of an Extended Kalman Filter for the plate temperature in heavy plate rolling", *Journal of Process Control*, 24, 9, 1371–1381, 2014. DOI: 10.1016/j.jprocont.2014.06.004
The content of this post-print version is identical to the published paper but without the publisher's final layout or copy editing.

$\Theta_j = \mathbf{h}_j(\mathbf{x}_j)$ is rather complicated, a simple empirical approximation of the form [23]

$$\Theta_j = k_1 T_j^{\mathrm{p,s}} + k_2 T_j^{\mathrm{p,s}} \left(\varepsilon^{\mathrm{p}} - \varepsilon_{\mathrm{pyro}}\right) + k_3 \left(\varepsilon^{\mathrm{p}} - \varepsilon_{\mathrm{pyro}}\right) + k_4 \tag{18}$$

with the constant coefficients $k_i, i = 1, \dots, 4$ can be derived for a pyrometer with the preset emissivity $\varepsilon_{\mathrm{pyro}}$. $T_j^{\mathrm{p,s}}$ denotes the actual surface temperature of the plate. If the emissivity ε^{p} is included in the model as a state using Eq. (8), the measurement equation (18) depends nonlinearly on the state because of the term $k_2 T_j^{\mathrm{p,s}} \varepsilon^{\mathrm{p}}$. Otherwise, it reduces to a simple affine relation.

Besides the pyrometer measurements of the upper and the lower temperature of the plate, no further measurements are available under normal production conditions. Consequently, the observer can only operate in open loop until the arrival of the next measurements.

3.4. Definition of covariance matrices

The standard deviation σ_j of the measurement can be used as an indicator of the quality of the measurement. Therefore, the covariance matrix $\mathbf{R}_j$ of the measurement noise $\mathbf{v}_j$ is defined as a function of σ_j. Furthermore, a reliability coefficient $r_{\mathrm{pyro}} > 0$ is assigned to each pyrometer. These coefficients are chosen based on experience and they capture, e. g., the respective measurement environment of the pyrometers. $\mathbf{R}_j$ is set to a diagonal matrix with the diagonal elements

$$R_j^{mm} = r_{\mathrm{pyro},m} \sigma_{j,m} \tag{19}$$

with $m = 1, \dots, 12$ referring to the pyrometer m.

To suitably define the covariance matrix $\mathbf{Q}_j$ of the process noise, the extended dynamic system (9) is analyzed. For the function $\mathbf{f}_j$, the process noise $\mathbf{w}_j = \left[\left(\mathbf{w}_j^{\mathrm{wr,lo}}\right)^T \left(\mathbf{w}_j^{\mathrm{p}}\right)^T \left(\bar{\mathbf{w}}_j^{\mathrm{wr,up}}\right)^T\right]$ is a disturbance of the temperature rate. To get an idea of the magnitude of $\mathbf{w}_j^{\mathrm{p}}$, the typical temperature rates $\dot{T}^{\mathrm{p},i}$ at different thickness coordinates y_i are considered in the various submodels, i. e., during air cooling periods, descaling passes and roll passes. The process noise $\mathbf{w}_j^{\mathrm{p}}$ is assumed to be proportional to these typical temperature rates. The proportionality factor depends on the assumed accuracy of the submodels. Consequently, the covariance of the process noise is set to

$$\begin{aligned} \mathbf{Q}_j^{\mathrm{p},k} &= E\left(\mathbf{w}_j^{\mathrm{p},k}\left(\mathbf{w}_j^{\mathrm{p},k}\right)^T\right) = \mathrm{diag}\left(\left[q^{\mathrm{p},k}(y_i)\right]\right) \\ k &\in \{\text{air, desc, cont}\}, \quad i = 1, \dots, N \end{aligned} \tag{20}$$

with the function

$$q^{\mathrm{p},k}(y_i) = r_{\mathrm{mod}}^k \left(\dot{T}^{\mathrm{p},i}\right)^2, \quad k \in \{\text{air, desc, cont}\} \tag{21}$$

and the coefficients $r_{\mathrm{mod}}^k > 0$. For example, the air cooling submodel is assumed to capture the reality with high accuracy so that the disturbance in the temperature rate is only small in the whole thickness domain. Thus, $r_{\mathrm{mod}}^{\mathrm{air}} > 0$ takes a small value. On the contrary, large disturbances in the rate of the surface temperature may occur during the descaling and the roll passes leading to larger coefficients $r_{\mathrm{mod}}^{\mathrm{desc}} > 0$ and $r_{\mathrm{mod}}^{\mathrm{cont}} > 0$.

The covariance matrices for the work rolls $\mathbf{Q}_j^{\mathrm{wr}}$ and $\bar{\mathbf{Q}}_j^{\mathrm{wr}}$ are determined analogously. The complete covariance matrix $\mathbf{Q}_j$ is assumed to be a block-diagonal matrix, i. e.,

$$\mathbf{Q}_j = \begin{pmatrix} \mathbf{Q}_j^{\mathrm{wr}} & \mathbf{0} & \mathbf{0} \\ \mathbf{0} & \mathbf{Q}_j^{\mathrm{p}} & \mathbf{0} \\ \mathbf{0} & \mathbf{0} & \bar{\mathbf{Q}}_j^{\mathrm{wr}} \end{pmatrix}. \tag{22}$$

By means of the matrix $\mathbf{Q}_j$, uncertainties in the material properties can also be taken into account. While the material properties, especially the heat capacity c_p, are well known for austenitic steel, large errors may arise in the temperature range of the phase transition. As the heat capacity strongly affects the temperature evolution, inaccurate heat capacity values may lead to large estimation errors. Therefore, the covariance of the process noise is set to a constant high value, i. e.,

$$q^{\mathrm{p},k}(y_i) = q_{\gamma \to \alpha}, \tag{23}$$

if the temperature drops into the range of the phase transition.

3.5. Recalculation of $\boldsymbol{P}_j$ at grid updates

During the roll passes, the plate thickness is reduced and consequently the spatial grid is deformed. To keep the spatial grid size approximately constant, which can be beneficial for the time integration process, the plate is remeshed after each roll pass. The temperature profile $\mathbf{x}_j^{\mathrm{p}}$ at the end of a pass is interpolated at the new grid points using spline interpolation resulting in the new state vector

$$\mathbf{x}_j \leftarrow \left[\left(\mathbf{x}_j^{\mathrm{wr,lo}}\right)^T \left(\mathbf{M}\mathbf{x}_j^{\mathrm{p}}\right)^T \left(\bar{\mathbf{x}}_j^{\mathrm{wr,up}}\right)^T\right]^T, \tag{24}$$

where the interpolation is expressed by the mapping matrix $\mathbf{M}$. The same mapping matrix $\mathbf{M}$ can be used to calculate the new covariance matrix given by

$$\mathbf{P}_j \leftarrow \widetilde{\mathbf{M}}\mathbf{P}_j\widetilde{\mathbf{M}}^T \quad \text{with} \quad \widetilde{\mathbf{M}} = \begin{pmatrix} \mathbf{I} & \mathbf{0} & \mathbf{0} \\ \mathbf{0} & \mathbf{M} & \mathbf{0} \\ \mathbf{0} & \mathbf{0} & \mathbf{I} \end{pmatrix}. \tag{25}$$

3.6. Reduced observer

In the reduced observer, the work rolls are only considered during the short contact periods with the plate, i. e., the work roll cooling is not simulated. This simplifies the simulation between two passes significantly because the number of states is reduced and a larger sampling time can be chosen.

Only during the contact periods, the state vector is extended by the states of both work rolls, i. e.,

$$\mathbf{x}_j = \begin{cases} \left[\left(\mathbf{x}_j^{\mathrm{wr,lo}}\right)^T \left(\mathbf{x}_j^{\mathrm{p}}\right)^T \left(\bar{\mathbf{x}}_j^{\mathrm{wr,up}}\right)^T\right]^T & \text{contact} \\ \mathbf{x}_j^{\mathrm{p}} & \text{else.} \end{cases} \tag{26}$$

At the beginning of each pass, the temperatures of the work rolls are set to $\mathbf{x}_j^{\mathrm{wr,lo}}(r) = \mathbf{x}_j^{\mathrm{wr,up}}(r) = 323\,\mathrm{K}$. This assumption is justified because the work rolls cool down to approximately room temperature between two passes due to the work

Post-print version of the article: K. Speicher, A. Steinboeck, A. Kugi, D. Wild, T. Kiefer, "Analysis and design of an Extended Kalman Filter for the plate temperature in heavy plate rolling", *Journal of Process Control*, 24, 9, 1371–1381, 2014. DOI: 10.1016/j.jprocont.2014.06.004
The content of this post-print version is identical to the published paper but without the publisher's final layout or copy editing.

roll cooling, see Fig. 3. The approach in (26) requires the covariance matrix $\mathbf{P}_j$ to be reorganized at the beginning and the end of each pass. At the beginning of a pass, the matrix $\mathbf{P}_j$ is built up using $\mathbf{P}_{j-1} = \mathbf{P}^{\mathrm{p}}_{j-1}$ calculated in the last time step before the pass and the constant matrices $\mathbf{P}^{\mathrm{wr}}_0$ and $\bar{\mathbf{P}}^{\mathrm{wr}}_0$. The extended covariance matrix takes the form

$$\mathbf{P}_j = \begin{pmatrix} \mathbf{P}^{\mathrm{wr}}_0 & \mathbf{0} & \mathbf{0} \\ \mathbf{0} & \mathbf{P}^{\mathrm{p}}_{j-1} & \mathbf{0} \\ \mathbf{0} & \mathbf{0} & \bar{\mathbf{P}}^{\mathrm{wr}}_0 \end{pmatrix}. \tag{27}$$

The block-diagonal structure of $\mathbf{P}_j$ indicates that the transient coupling between the estimation errors of the temperatures of the plate and the work rolls due to the preceding roll passes can be neglected. At the end of each pass, only the central block of $\mathbf{P}_j$ is preserved to give a starting value for the subsequent air cooling period, i. e.,

$$\mathbf{P}_j = \begin{pmatrix} \mathbf{P}^{\mathrm{wr}}_j & \mathbf{P}^{\mathrm{wr,p}}_j & \mathbf{P}^{\mathrm{wr,wr}}_j \\ \mathbf{P}^{\mathrm{p,wr}}_j & \mathbf{P}^{\mathrm{p}}_j & \bar{\mathbf{P}}^{\mathrm{p,wr}}_j \\ \mathbf{P}^{\mathrm{wr,wr}}_j & \bar{\mathbf{P}}^{\mathrm{wr,p}}_j & \bar{\mathbf{P}}^{\mathrm{wr}}_j \end{pmatrix} \rightarrow \mathbf{P}_{j+1} = \mathbf{P}^{\mathrm{p}}_j. \tag{28}$$

All other blocks of the covariance matrix — the ones corresponding to one work roll ($\mathbf{P}^{\mathrm{wr}}_j, \bar{\mathbf{P}}^{\mathrm{wr}}_j$) and the cross-covariances ($\mathbf{P}^{\mathrm{wr,p}}_j, \mathbf{P}^{\mathrm{wr,wr}}_j, \bar{\mathbf{P}}^{\mathrm{wr,p}}_j$) — are discarded. Consequently, the reduced observer focuses only on the temperature profile $\mathbf{x}^{\mathrm{p}}_j$ of the plate and its estimation error covariance matrix $\mathbf{P}^{\mathrm{p}}_j$. This reduction of the system is the only difference between the full and the reduced observer.

Concerning the covariance matrices, the considerations of the previous section are still valid. However, $\mathbf{Q}_j$ is extended at the beginning of each pass and reduced at the end of each pass in a similar way as $\mathbf{P}_j$, see Eq. (27) and (28).

4. Results

In this section, the developed EKF is validated by means of experimental data. In Section 4.1, measurements of the temperature inside an instrumented test plate are used for this purpose. As the test plate is not rolled, the modeled interaction between the work rolls and the plate cannot be verified by means of this setting. This interaction effect is validated in Section 4.2 based on the measurements of a plate from the normal production. There, the full observer and the reduced one are compared in terms of the estimated temperatures and their computational load.

4.1. Experimental validation of the EKF

4.1.1. Experimental setup

To validate the EKF, an experiment was carried out at the industrial rolling mill of the AG der Dillinger Hüttenwerke. A 42 mm thick test plate was instrumented with thermocouples at the coordinates $y = 4$ mm, $y = 21$ mm, and $y = 38$ mm so that the temperature could also be measured inside the plate. The plate was heated up in a furnace to approximately 1100 K. After a short air cooling period, the plate was descaled. In total, five descaling passes with subsequent air cooling periods were performed leading to a final temperature below 900 K. During the whole experiment, the surface temperatures were regularly measured by pyrometers.

As the experiment covered only air cooling periods and descaling passes, no coupling of the plate and the work rolls has to be considered. Consequently, the full and the reduced observer do not differ from each other for this experiment. Hence, this section focuses on the verification of the estimated temperature profile when only measurements of the surface temperature are fed into the EKF. These are the measurements that are also available during the normal production process. Furthermore, in addition to the temperature, the emissivity of the plate is also estimated according to (8).

4.1.2. Experimental results

Figure 5 shows a comparison of the estimated surface and core temperatures, $\hat{T}^{\mathrm{p,s}}$ and $\hat{T}^{\mathrm{p,c}}$, respectively, with the pyrometer measurements $\Theta^{\mathrm{p,s}}$. There is only one bottom-side pyrometer behind the finishing mill so that measurements of the temperature of the lower surface (gray dots in Fig. 5) are available only in the second half of the experiment. For clarity reasons, the difference $\Delta T^{\mathrm{p,s}}$ between the estimated and the measured surface temperatures is given in Fig. 6. The observed temperature error generally is of the order ±10 K. Larger errors occur shortly after the third and the fourth descaling pass. They may be caused by measurements which are faulty because the water of the descaler sprays streams on the plate surface.

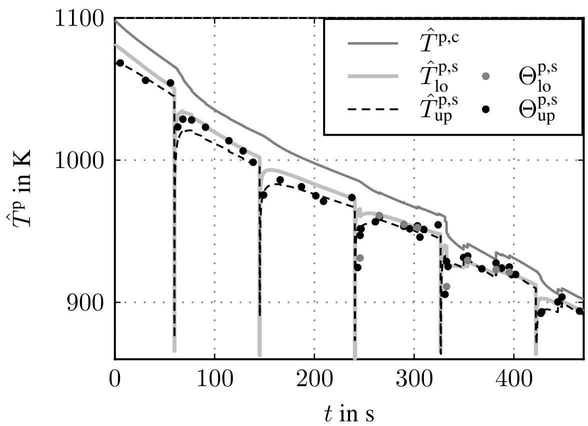

Figure 5: Comparison of the estimated surface and core temperatures with the pyrometer measurements.

After the first descaling pass, an almost constant error of $\Delta T^{\mathrm{p,s}} = -8$ K can be observed. At the same time, the emissivity $\hat{\varepsilon}^{\mathrm{p}}$ estimated by the EKF is strongly increased in response to the observed surface temperature error, see Fig. 7. The observed increase in the emissivity after the first descaling pass confirms the results presented in [1], where the values $\varepsilon^{\mathrm{p}} = 0.65$ and $\varepsilon^{\mathrm{p}} = 1$ were identified for the scaled and the descaled plate, respectively.

A potential weakness of the proposed parameter estimation strategy is that an observed surface temperature error can be

Post-print version of the article: K. Speicher, A. Steinboeck, A. Kugi, D. Wild, T. Kiefer, "Analysis and design of an Extended Kalman Filter for the plate temperature in heavy plate rolling", *Journal of Process Control*, 24, 9, 1371–1381, 2014. DOI: 10.1016/j.jprocont.2014.06.004

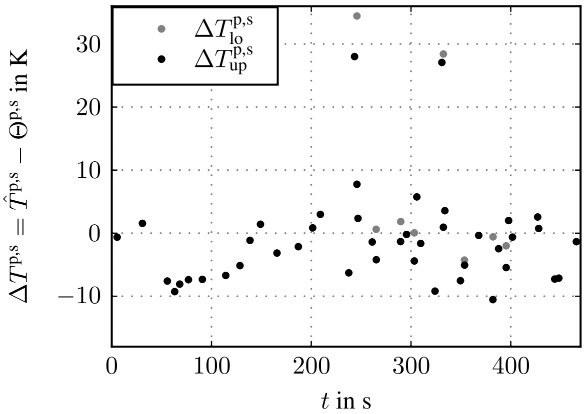

Figure 6: Difference between the estimated surface temperatures and the pyrometer measurements.

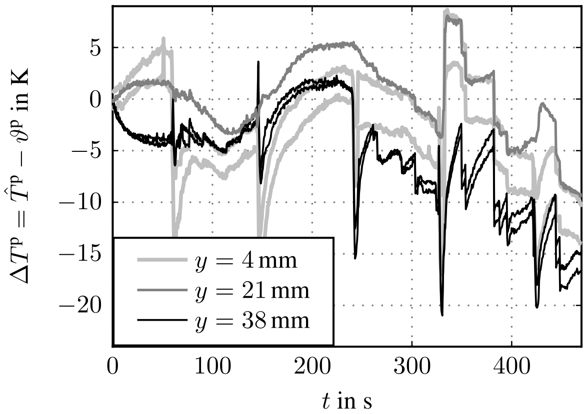

Figure 8: Difference between the estimated temperatures and the thermocouple measurements.

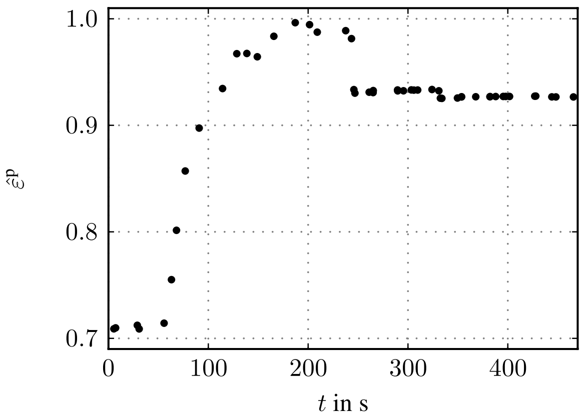

Figure 7: Emissivity of the plate estimated by the EKF.

caused either by an error in the estimated surface temperature or by a wrong emissivity according to Eq. (18). A reliable attribution of possible surface temperature errors to one of those effects seems rather difficult based on the existing measurement facilities. The result of the EKF strongly depends on the choice of the covariance matrices $\mathbf{P}_0$ and $\mathbf{Q}_j$.

Fig. 6 shows that the estimation error scatters with respect to its mean value. The scattering of the order ± 10 K can be mainly attributed to two causes: First, the measurements are recorded by different pyrometers which are calibrated with a calibration tolerance of ± 6 K. Second, the measurement accuracy of the radiation pyrometers is 1% of the measurement range which also corresponds to approximately ± 6 K. Bearing in mind these inaccuracies and the challenging measurement conditions (dirt and water on the plate surface, steam in the proximity of the mill stands), the agreement between the estimated temperatures $\hat{T}^{p}$ and the thermocouple measurements ϑ^{p} is satisfactory during the first 300 s of the experiment, cf. Fig. 8. At the end of the experiment, the estimated temperatures and the thermocouple measurements drift apart from each other because the pyrometer measurements do not match the thermocouple measurements anymore. This discrepancy between the temperatures recorded by the pyrometers and the thermocouples may arise from the low temperature at the end of the experiment. The surface temperature is close to the lower limit of the measuring range of the pyrometers, where the pyrometer readings are typically more noisy and less reliable. It is again emphasized that the estimated states are only updated based on infrequent and possibly disturbed pyrometer measurements, whereas the continuous thermocouple measurements are just used for verification.

The largest deviations between the estimated and the measured temperatures occur shortly after the descaling passes and close to the plate surfaces. This observation confirms the assumptions about the process noise discussed in Section 3.4. From the fourth descaling pass onwards, the corrections of the EKF are stronger than at the beginning of the experiment. By then, the plate cooled down to the temperature range in which the phase transition takes place. Consequently, the covariance matrix of the process noise is increased, see Eq. (23), and the covariance matrix of the estimation error grows according to Eq. (15) leading to a larger Kalman gain, cf. Eq. (11).

It can be concluded that the developed EKF provides good estimations of the plate temperature profile using infrequent pyrometer measurements of the surface temperature. Furthermore, the plate emissivity can be estimated although the surface conditions change during the experiment leading to an increase of the emissivity.

4.2. *Comparison of the full and the reduced EKF*

The previously presented experiment did not include roll passes so that neither the coupling effect between the work rolls and the plate nor the differences between the full observer and the reduced one could be investigated. To analyze this coupling effect, the production of a standard plate is considered in the following. The plate was rolled in 17 passes to a final thickness of 12 mm. After each pass, at least two pyrometer measurements of the temperature of the upper plate surface were recorded. Measurements of the lower surface temperature are only available at the finishing mill.

As already discussed in Section 2.2, the plate and the work rolls are coupled only during the short contact time during the

Post-print version of the article: K. Speicher, A. Steinboeck, A. Kugi, D. Wild, T. Kiefer, "Analysis and design of an Extended Kalman Filter for the plate temperature in heavy plate rolling", *Journal of Process Control*, 24, 9, 1371–1381, 2014. DOI: 10.1016/j.jprocont.2014.06.004
The content of this post-print version is identical to the published paper but without the publisher's final layout or copy editing.

passes. Due to the contact, the work rolls heat up in the outer shell. Between two passes, they cool down to approximately the same temperature as before the pass, see Fig. 3. Therefore, it can be assumed that the work roll has the same homogeneous temperature profile at the beginning of each pass. However, the evolution of the covariance matrix and thus the corrections by the observer may be influenced by the temporary coupling of the work rolls and the plate. To investigate this influence, the full observer and the reduced observer are compared concerning their estimations of the temperature profile as well as regarding their estimation error covariance matrices.

4.2.1. Comparison of the covariance matrices

In the following, the covariance matrices calculated by both observers are compared. As an example, the fifth roll pass is considered because the coupling of the plate and the work rolls would have already led to visible differences at this point if it was significant. Figs. 9 and 10 show the covariance matrices at the beginning and the end, respectively, of the fifth roll pass computed by the full observer.

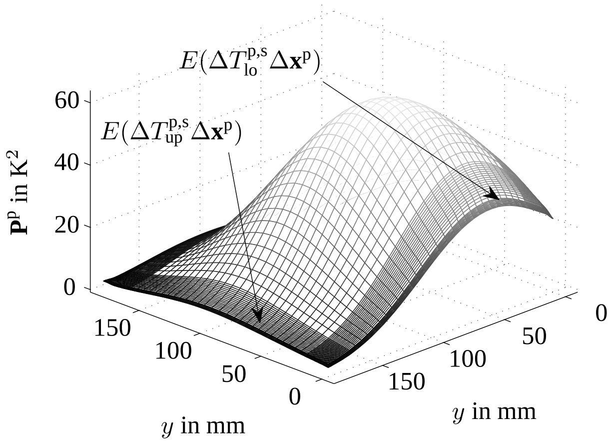

Figure 9: Covariance matrix of the estimation error of the plate at the beginning of the fifth roll pass (full observer).

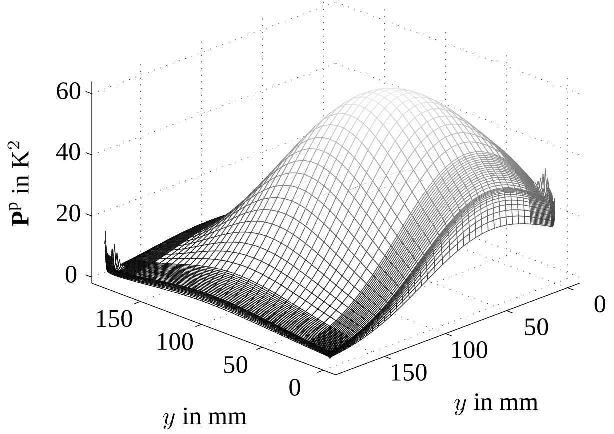

Figure 10: Covariance matrix of the estimation error of the plate at the end of the fifth roll pass (full observer).

While the estimation error in the lower half of the plate is still large, the states close to the upper surface are estimated with higher accuracy, cf. the expectations $E(\Delta T_{\mathrm{lo}}^{\mathrm{p,s}} \Delta \mathbf{x}^{\mathrm{p}})$ and $E(\Delta T_{\mathrm{up}}^{\mathrm{p,s}} \Delta \mathbf{x}^{\mathrm{p}})$ shown in Fig. 9. The better estimation accuracy close to the upper surface can be explained by the fact that ten measurements of the upper surface temperature were used for corrections up to the fifth pass. On the contrary, no measurement information about the lower surface temperature was available during this period.

The roll passes mainly affect the estimation error covariance at grid points close to the surfaces. Therefore, $\mathbf{P}^{\mathrm{p}}$ barely changes during the roll pass apart from the rows and columns corresponding to these outer grid points. As the coupling of the plate and the work rolls has the strongest influence on these grid points, the two observers clearly exhibit the largest differences there. This supposition is confirmed by Figs. 11 and 12,

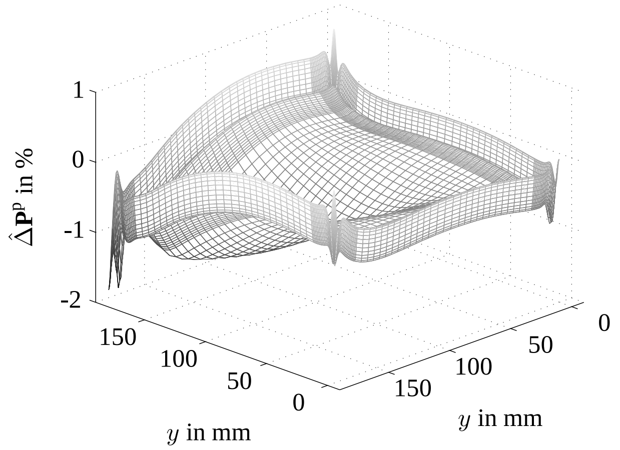

Figure 11: Deviation of the covariance matrices of the estimation error of the plate at the beginning of the fifth roll pass (full vs. reduced observer).

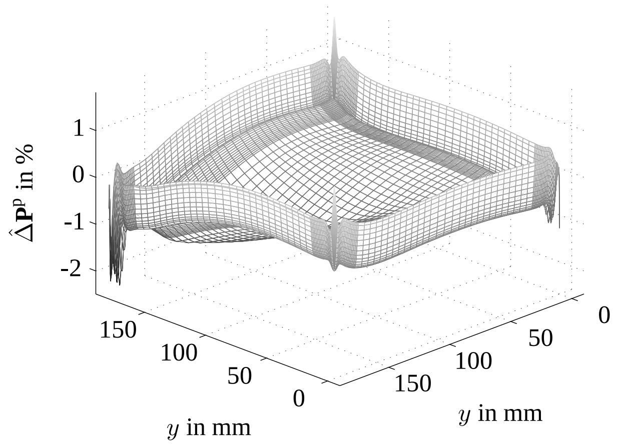

Figure 12: Deviation of the covariance matrices of the estimation error of the plate at the end of the fifth roll pass (full vs. reduced observer).

where the relative deviation between the observers is shown. Although the observers deviate more strongly close to the surfaces, the difference between both observers is small.

Post-print version of the article: K. Speicher, A. Steinboeck, A. Kugi, D. Wild, T. Kiefer, "Analysis and design of an Extended Kalman Filter for the plate temperature in heavy plate rolling", *Journal of Process Control*, 24, 9, 1371–1381, 2014. DOI: 10.1016/j.jprocont.2014.06.004
The content of this post-print version is identical to the published paper but without the publisher's final layout or copy editing.

The increase in the deviation during the roll pass can be attributed to the initialization of the cross-covariances $\mathbf{P}^{\mathrm{wr,p}}$ and $\bar{\mathbf{P}}^{\mathrm{p,wr}}$ with zero matrices at the beginning of a pass in the reduced observer, cf. (27). Even if the cross-covariances are small, see Fig. 13, they contribute to the evolution of $\mathbf{P}^{\mathrm{p}}$. During a pass,

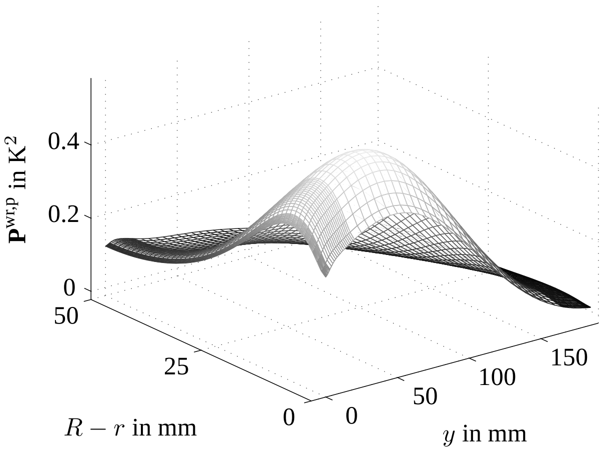

Figure 13: Cross-covariance matrix of the estimation error at the beginning of the fifth roll pass (full observer).

the elements of the cross-covariances corresponding to both the plate and the work roll surface grow fast, see Fig. 14. However, all other elements in $\mathbf{P}^{\mathrm{wr,p}}$ and $\bar{\mathbf{P}}^{\mathrm{p,wr}}$ remain practically unaffected because the contact time is short so that heat diffusion does not reach the subsurface regions of the material. When the

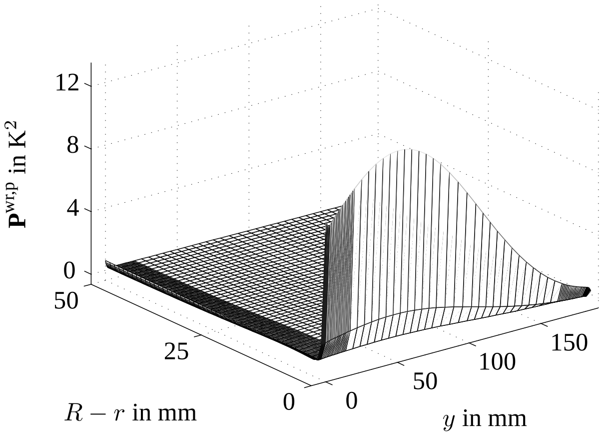

Figure 14: Cross-covariance matrix of the estimation error at the beginning of the fifth roll pass (full observer).

plate and the work rolls are decoupled during the subsequent air cooling period, the cross-covariances homogenize. However,their elements are still small compared to those of $\mathbf{P}^{\mathrm{p}}$, compare Figs. 9 and 13, so that the initial values defined in Eq. (27) are tenable.

In summary, the reduced observer leads to approximately the same estimation error covariance matrices as the full observer. In the following section, the two observers are compared in terms of the estimated temperature profile.

4.2.2. Comparison of the temperature fields

The temperature evolution calculated by the full observer is shown in Fig. 15. After the descaling in the descaler unit, the first measurement of the temperature of the upper surface indicates that the estimated temperature is approximately 20 K too high. Consequently, the whole temperature profile is significantly corrected. Here, the observer benefits from the systematic design of $\mathbf{P}_0^{\mathrm{p}}$ (cf. Sec. 3.2). As the covariance matrix of the estimation error is a dense matrix, the correction affects not only the surface temperature but also the other states. The following measurements at the roughing mill confirm this correction behavior. Compared to the first update of the temperature profile, all other corrections are rather small. Because of the correction, the covariance of the estimation error also decreases strongly, cf. Figs. 4 and 9.

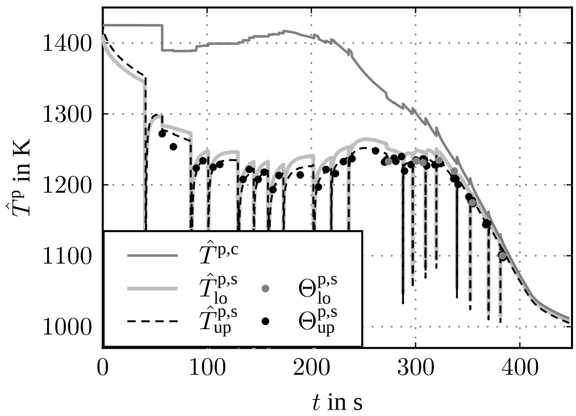

Figure 15: Comparison of the estimated surface and core temperatures of the plate with the pyrometer measurements (full observer).

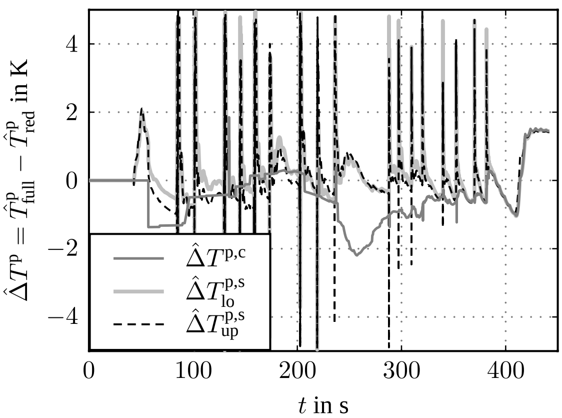

Figure 16: Difference in the estimated surface and core temperatures of the plate (full vs. reduced observer).

Figure 16 shows the differences in the temperature evolution estimated by the two observers. The largest deviations occur during the contact with the work rolls and immediately afterwards. However, they decrease quickly so that the remaining difference between the observers is within ±2 K.

The good agreement of both observers and the pyrometer

Post-print version of the article: K. Speicher, A. Steinboeck, A. Kugi, D. Wild, T. Kiefer, "Analysis and design of an Extended Kalman Filter for the plate temperature in heavy plate rolling", *Journal of Process Control*, 24, 9, 1371–1381, 2014. DOI: 10.1016/j.jprocont.2014.06.004

measurements can also be seen in Fig. 17, where the estimation errors of the surface temperatures are given. The mean value of the estimation error is indeed small, but the estimation error scatters approximately ±10 K with respect to its mean value. This scattering and its causes were discussed in Sec. 4.1. Furthermore, Fig. 17 shows that the estimation ac-

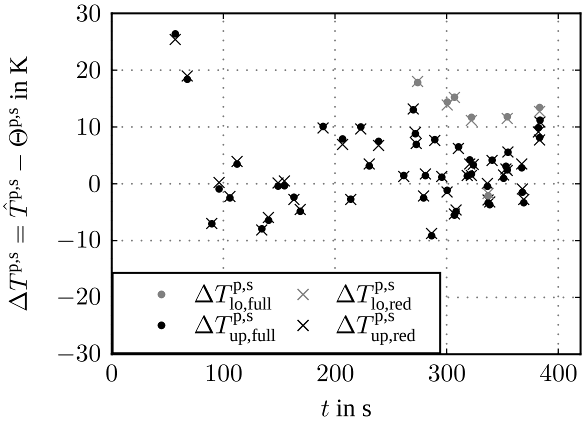

Figure 17: Comparison of the estimated surface temperatures of the plate with the pyrometer measurements (full and reduced observer).

curacy achieved at the upper surface is superior compared to the lower surface. However, the measurements of the temperature of the lower surface are less reliable because they may be disturbed by dropping water or dirt. Further problems may be caused by the approximate measurement equation (18) whose derivation is more complicated for measurements of the lower surface temperature. The radiation incident on a bottom-side pyrometer and thus the measured temperature depend not only on the unknown radiative properties of the plate as discussed in Sec. 3.3. It may also contain radiative energy emitted or reflected by the roller table and consequently depend on the emissivity, the temperature, and also the geometry of the roller table, see [23]. These factors cannot be properly captured by Eq. (18) and lead to a higher degree of uncertainty in the lower surface temperature measurements.

In summary, the reduced observer leads to practically the same results as the full observer in terms of the estimated temperature evolution as well as the covariance of the estimation error. As the state vector and the estimation error covariance matrix are easily adaptable, see (26) – (28), neglecting the work roll cooling between two passes does not pose any problem. Moreover, this reduced model simplifies the simulation. The influence of the reduction on the computing time is discussed in the following section.

4.2.3. Comparison of the computational load

For the investigated plate, the reduction of the system during the air cooling periods decreases the system dimension by more than 50%, see Tab. 1. Initially, the plate grid consists of 91 grid points. Hence, the temperatures of the 102 grid points of the upper and the lower work roll are the majority of the states already at the beginning of the production process. When the number of plate grid points decreases in the course of the production due to the reduced thickness, almost three quarters of the states correspond to the work rolls. Therefore, the computation can

maximum number of plate grid points	91
minimum number of plate grid points	37
number of grid points per work roll	51

Table 1: Number of grid points.

be greatly sped up from 27.34 s to 4.77 s, see Tab. 2, when the reduced observer is used. These computing times refer to the calculation of the whole production process of the plate which is presented in Fig. 15 and takes approximately 450 s.

full EKF	27.34 s	100%
reduced EKF	4.77 s	17.45%

Table 2: Computing time for the whole production process (450 s).

The time discretization of both observers is chosen by a time step adaptation algorithm. This algorithm automatically reduces the time step if the heat flux leaving the plate exceeds a given limit or if the boundary condition switches. As the boundary condition of the work rolls often switches, small time steps are required by the full observer. In contrast, the reduced observer can also use larger time steps during the air cooling periods. This also leads to the observed speed-up of the calculation.

The computing times given in Tab. 2 were obtained when executing the observers realized in Matlab on a standard desktop computer (Intel Core 2, 2.4 GHz, 6 GB RAM). Further improvements can be achieved by implementation in a general-purpose programming language like C or by optimization of the spatial and time discretization. As the computing time is much smaller than the production time, the observers can be implemented in real time.

5. Conclusions and outlook

In this paper, an Extended Kalman Filter for the plate temperature in heavy plate rolling was presented. The initialization and the parametrization of the EKF were discussed in detail. The parameter tuning was demonstrated for the specific application of hot rolling, but the adopted strategy may also be useful for other applications. The performance of the observer was assessed by means of extensive experimental data. The observer shows a very good estimation accuracy although only few measurements of the surface temperature are available and all other states are not measurable under normal production conditions. Besides the estimation of the plate temperature, a possible estimation of the emissivity of the plate by the EKF was also discussed. It was shown that a simultaneous estimation of the temperatures and the emissivity is feasible and yields good results.

Furthermore, the coupling effect between the plate and the work rolls was investigated. In the considered case of heavy plate rolling, it is admissible to consider the work rolls only when they are in contact with the plate. This reduced observer

Post-print version of the article: K. Speicher, A. Steinboeck, A. Kugi, D. Wild, T. Kiefer, "Analysis and design of an Extended Kalman Filter for the plate temperature in heavy plate rolling", *Journal of Process Control*, 24, 9, 1371–1381, 2014. doi: 10.1016/j.jprocont.2014.06.004
The content of this post-print version is identical to the published paper but without the publisher's final layout or copy editing.

yields almost the same results as the full observer, but it is computationally more efficient due to the simplified structure and the reduced number of states. Similar reduced observers may also be useful for other temporarily coupled systems if the coupling time is significantly smaller than the time during which the systems are decoupled. In general, this is the case for many products fabricated in assembly line production. For such systems, the contact times between the tools and the work pieces are usually short compared to the total production time. Moreover, the system dynamics and the way of coupling may play an important role. In the considered case, the coupling of the plate and the work rolls influences mainly the areas of the plate which are close to the surfaces. If, however, the coupling influences the whole system already during a short coupling time, as, e. g., in strip rolling, the development of a reduced observer may not be possible.

The scarcity of available measurements poses a major challenge for the EKF. Therefore, future work will focus on the optimization of the measurement facilities. The optimal placement of the pyrometers will be investigated so that a maximum number of high quality measurements is recorded. Furthermore, it has to be analyzed how other measured quantities which depend on the temperature, e. g., the rolling force, can be utilized by the EKF.

Acknowledgments

The second author highly appreciates financial support provided by the Austrian Academy of Sciences in the form of an APART-fellowship at the Automation and Control Institute of Vienna University of Technology.

References

[1] K. Speicher, A. Steinboeck, D. Wild, T. Kiefer, A. Kugi, An integrated thermal model of hot rolling, Mathematical and Computer Modelling of Dynamical Systems 20 (1) (2014) 66–86.

[2] R. Colas, Modelling heat transfer during hot rolling of steel strip, Modelling and Simulation in Materials Science and Engineering 3 (1995) 437–453.

[3] C. Devadas, I. Samarasekera, Heat transfer during hot rolling of steel strip, Ironmaking and Steelmaking 13 (1986) 311–321.

[4] D. Jin, V. Hernandez-Avila, I. Samarasekera, J. Brimacombe, An integrated process model for the hot rolling of plain carbon steel, in: J. Beynon, P. Ingham, H. Teichert, K. Waterson (Eds.), Proceedings of the 2nd International Conference on Modelling of Metal Rolling Processes, Institute of Materials, London, UK, 1996, pp. 36–58.

[5] K. Yanagi, Prediction of strip temperature for hot strip mills, Transactions of the Iron and Steel Institute of Japan 16 (1) (1976) 11–19.

[6] S. Zhou, An integrated model for hot rolling of steel strips, Journal of Materials Processing Technology 134 (3) (2003) 338–351.

[7] P. Atack, I. Robinson, Adaptation of hot mill process models, Journal of Materials Processing Technology 60 (1–4) (1996) 535–542.

[8] R. Stephens, A. Randall, On-line adaptive control in the hot rolling of steel, Control Theory and Applications, IEE Proceedings 144 (1) (1997) 15–24.

[9] Y. Zheng, S. Li, Plant-wide temperature drop monitoring in run-out table strip cooling process, in: Proceedings of the International Symposium on Advanced Control of Industrial Processes (ADCONIP), Hangzhou, China, 2011, pp. 287–292.

[10] A. Alessandri, P. Coletta, Design of Luenberger observers for a class of hybrid linear systems, in: M. Benedetto, A. Sangiovanni-Vincentelli (Eds.), Hybrid Systems: Computation and Control, Vol. 2034 of Lecture Notes in Computer Science, Springer Berlin Heidelberg, 2001, pp. 7–18.

[11] A. Alessandri, M. Baglietto, G. Battistelli, A maximum-likelihood Kalman filter for switching discrete-time linear systems, Automatica 46 (11) (2010) 1870–1876.

[12] G. Goffaux, A. Vande Wouwer, O. Bernard, Continuous - discrete interval observers for monitoring microalgae cultures, Biotechnology Progress 25 (3) (2009) 667–675.

[13] D. Dochain, State and parameter estimation in chemical and biochemical processes: a tutorial, Journal of Process Control 13 (8) (2003) 801–818.

[14] S. Bolognani, L. Tubiana, M. Zigliotto, Extended kalman filter tuning in sensorless pmsm drives, IEEE Transactions on Industry Applications, 39 (6) (2003) 1741–1747.

[15] M. Boutayeb, D. Aubry, A strong tracking extended kalman observer for nonlinear discrete-time systems, IEEE Transactions on Automatic Control 44 (8) (1999) 1550–1556.

[16] H. D. Baehr, K. Stephan, Heat and mass transfer, 2nd Edition, Springer Berlin Heidelberg, 2006.

[17] S. Serajzadeh, F. Mucciardi, Modelling the work-roll temperature variation at unsteady state condition, Modelling and Simulation in Materials Science and Engineering 11 (2) (2003) 179–194.

[18] T. Larsen, N. Andersen, O. Ravn, N. Poulsen, Incorporation of time delayed measurements in a discrete-time Kalman filter, in: Proceedings of the 37th IEEE Conference on Decision and Control, Vol. 4, Tampa, USA, 1998, pp. 3972–3977.

[19] S. C. Thomopoulos, L. Zhang, Decentralized filtering with random sampling and delay, Information Sciences 81 (1-2) (1994) 117–131.

[20] A. Gopalakrishnan, N. S. Kaisare, S. Narasimhan, Incorporating delayed and infrequent measurements in extended Kalman filter based nonlinear state estimation, Journal of Process Control 21 (1) (2011) 119–129.

[21] D. Wild, T. Meurer, A. Kugi, Modelling and experimental model validation for a pusher-type reheating furnace, Mathematical and Computer Modelling of Dynamical Systems 15 (3) (2009) 209–232.

[22] K. Speicher, A. Steinboeck, D. Wild, T. Kiefer, A. Kugi, Estimation of plate temperatures in hot rolling based on an extended Kalman filter, in: Proceedings of the 15th IFAC Symposium on Control, Optimization and Automation in Mining, Minerals and Metal Processing, Vol. 15, San Diego, USA, 2013, pp. 409–414.

[23] K. Speicher, A. Steinboeck, A. Kugi, D. Wild, T. Kiefer, Measurement errors of radiation pyrometers and their corrections, in: CD-Proceedings of the 9th International and 6th European Rolling Conference, Venice, Italy, 2013, p. 12.

Post-print version of the article: K. Speicher, A. Steinboeck, A. Kugi, D. Wild, T. Kiefer, "Analysis and design of an Extended Kalman Filter for the plate temperature in heavy plate rolling", *Journal of Process Control*, 24, 9, 1371–1381, 2014. DOI: 10.1016/j.jprocont.2014.06.004
The content of this post-print version is identical to the published paper but without the publisher's final layout or copy editing.